Article

Effect of Annealing on the Thermoelectricity Properties of the WRe26-In$_2$O$_3$ Thin Film Thermocouples

Bian Tian [1],*, Yan Liu [1],* , Zhongkai Zhang [1], Zhaojun Liu [1], Libo Zhao [1], Qijing Lin [1], Peng Shi [2], Qi Mao [1], Dejiang Lu [1] and Zhuangde Jiang [1]

[1] State Key Laboratory for Mechanical Manufacturing Systems Engineering, Xi'an Jiaotong University, Xi'an 710049, China; z.zhongkai@stu.xjtu.edu.cn (Z.Z.); lzj2018@stu.xjtu.edu.cn (Z.L.); libozhao@mail.xjtu.edu.cn (L.Z.); qjlin2015@mail.xjtu.edu.cn (Q.L.); mq.mq@xjtu.edu.cn (Q.M.); djlu@xjtu.edu.cn (D.L.); zdjiang@mail.xjtu.edu.cn (Z.J.)

[2] Electronic Materials Research Laboratory, Key Laboratory of the Ministry of Education & International Center for Dielectric Research, Xi'an Jiaotong University, Xi'an 710049, China; spxjy@xjtu.edu.cn

* Correspondence: t.b12@mail.xjtu.edu.cn (B.T.); liuyanzj402@stu.xjtu.edu.cn (Y.L.)

check for updates

Abstract: WRe26-In$_2$O$_3$ (WRe26 (tungsten-26% rhenium) and In$_2$O$_3$ thermoelectric materials) thin film thermocouples (TFTCs) have been fabricated based on magnetron sputtering technology, which can be used in temperature measurement. Many annealing processes were studied to promote the sensitivity of WRe26-In$_2$O$_3$ TFTCs. The optimal annealing process of the thermocouple under this kind of RF magnetron sputtering method was proposed after analyzing the properties of In$_2$O$_3$ films and the thermoelectric voltage of TFTCs at different annealing processes. The calibration results showed that the WRe26-In$_2$O$_3$ TFTCs achieved a thermoelectric voltage of 123.6 mV at a temperature difference of 612.9 K, with a sensitivity of up to 201.6 µV/K. Also, TFTC kept a stable thermoelectric voltage output at 973 K for 20 min and at 773 K for two hours. In general, the WRe26-In$_2$O$_3$ TFTCs developed in this work have great potential for practical applications. In future work, we will focus on the thermoelectric stability of TFTCs at higher temperatures.

Keywords: WRe26-In$_2$O$_3$ thin films; thermocouples; annealing; magnetron sputtering

1. Introduction

The accurate measurement of high temperature is particularly important in modern science. With the development of MEMS technology, TFTCs are widely used in many areas [1–4]. TFTCs have many advantages, such as fast response, high measurement accuracy, and easy integration [5–7]. Traditionally, for metal TFTCs, Such as type-K (Ni$_{10}$Cr/Ni$_5$Si) and type-S (Pt-10%Rh/Pt) TFTCs [8–11]. This kind of metal TFTCs have low sensitivity and low thermoelectric voltage output. To achieve high sensitivity and oxidation resistance, some silicide, carbides, and conductive oxides have been developed as alternative electrodes for high temperature measurement, such as the working temperature of CrSi$_2$-TaC TFTCs in a vacuum or inert gas going up to 1080 °C while the thermoelectric output remains stable. When it was in an oxidizing atmosphere, it failed at 455 °C. Meanwhile, CrSi$_2$ can only work stably in an oxidizing environment at 670 °C; for more than 180 h, its sensitivity coefficient is 102 µV/°C [12,13]. MoSi$_2$-TiSi$_2$ carbide TFTCs was used to high temperature of 1200 °C. However, at high temperatures, SiO$_2$ is formed due to oxygen entering the film, which leads the stability of the TFTCs to become worse due to the composition of the thin-film changes [14]. Compared to carbide and silicide thin film thermocouples, oxide ceramic TFTCs have more potential for high temperature

stability and thermoelectric voltage output. Indium tin oxide (ITO) as a prevalent conductive oxide has been applied to TFTCs [15–17].

The basic principle of the thermocouple is based on the Seebeck effect, wherein two legs of the thermocouple have different Seebeck coefficients. Also, most of the metal and semiconductor thermoelectric materials are the same type. That is, the Seebeck coefficients of thermoelectric materials are all positive or negative. The Seebeck coefficients of tungsten-rhenium TFTCs are both positive, and the Seebeck coefficients of In_2O_3-ITO thermoelectric materials are negative. In order to increase the sensitivity of the TFTCs, one Seebeck coefficient of thermoelectric material is negative, while another, which is positive, is chosen. Therefore, some metal-oxide TFTCs are developed. Platinum (Pt) is a refractory precious metal with a low Seebeck coefficient and higher oxidation resistance, which can be used as a leg of TFTCs, such as Pt-ITO, Pt-ITON and Pt-In_2O_3 TFTCs [18–20]. During the heating cycle of 25–1200 °C, the Pt-ITO showed good stability; its Seebeck coefficient was up to 65.39 μV/°C [21]. Oxide (ITO) is annealed in a nitrogen atmosphere to improve the thermoelectricity stability of the Pt-ITON TFTCs.

It is hoped that prepared TFTCs have strong high temperature resistance and a high thermoelectric voltage output. The tungsten-rhenium TFTCs have been reported for high temperature measurements of up to about 1500 °C [22–24]. Typical In_2O_3-ITO TFTCs have been reported which have shown a higher thermoelectric voltage output (173 mV at 1273 °C) and high temperature stability. To obtain high temperature resistance and high thermoelectric voltage output at the same time, WRe26 and In_2O_3 are chosen as a new combination of TFTCs based on the SI_3N_4 substrate. In this paper, the WRe26-In_2O_3 TFTCs were fabricated by RF magnetron sputtering, and the proprieties of In_2O_3 thin films and the thermoelectric voltage output of the TFTCs were analyzed under different annealing processes. The best annealing process was found to make the sensitivity of the WRe26-In_2O_3 TFTCs reach the expectation.

2. Theoretical Analysis

The principle of TFTCs are the same as the traditional wire thermocouples, which is based on the Seebeck effect [25,26]. When the hot junction is heated, and its temperature is T_1. And the temperature of cold junction is T_0. The thermoelectric potential can be measured at the cold junction of the thermocouples. The thermoelectric voltage of the thin film thermocouple is described as:

$$E_{AB} = \int_{\theta_0}^{\theta} S_{AB}(T)dT = \int_{\theta_0}^{\theta} [S_B(T) - S_A(T)]dT \qquad (1)$$

where the $S_{AB}(T)$ is the Seebeck coefficient of TFTC, $S_A(T)$ is the Seebeck coefficient of material A; $S_B(T)$ is the Seebeck coefficient of material B, θ is the temperature of hot junction; θ_0 is temperature of cold junction.

At the same time, the Seebeck coefficient of the conductive oxides are different from the metals. In_2O_3 is an N-type non-degenerate semiconductor material. The Seebeck coefficient of In_2O_3 is gave as:

$$S(N_D) = -\frac{Ak}{e} - \frac{k}{e}In\left(\frac{(2\pi m_e^* kT)^{2/3}}{h^3 N_D}\right) \qquad (2)$$

where S is Seebeck coefficient, K is the Boltzmann constant, h is the Planck constant, e respects electronic charges; N_D is carrier concentration, m_e is effective mass, A is a transport constant [27]. If additional oxygen enters the In_2O_3, it will affect the Seebeck coefficient of the In_2O_3. The conductive carriers of In_2O_3 mainly comes from the electrons released by the oxygen vacancy, and one oxygen vacancy contributes two electrons (Equation (3)) [28]. V_O are doubly charged oxygen vacancies. When additional

oxygen occupied the oxygen vacancy of the In_2O_3 film, it caused the carrier concentration in the In_2O_3 film to decrease while increasing the Seebeck coefficient of the In_2O_3.

$$O_o^x \rightarrow 1/2O_2 + V_O + 2e^{-1} \tag{3}$$

To verify whether the thermoelectric voltage output of WRe26-In_2O_3 was better than the pure oxide combination (ITO-In_2O_3), thermoelectricity simulation of TFTCs with different thermoelectric material combinations was required. The thermoelectric characteristics of the ITO-WRe26, WRe26-In_2O_3 and ITO-In_2O_3 TFTCs were studied by using commercial software COMSOL to ensure the results of model analysis. Figure 1 shows the model of the three combinations of TFTCs. The single size of the TFTC is 30 mm × 90 mm. The area of hot junctions is 4 mm × 10 mm. In this analysis, the temperature of hot junctions was increased from 300 K to 1300 K, and the cold junctions were set to 293 K. The Finite Element Analysis results of temperature gradient and thermoelectric voltage distribution are presented in Figure 2. The maximum temperature of the hot junctions are 1300 K. Figure 3 shows the thermoelectric voltage output of TFTCs. According to the simulation results, thermoelectric output of WRe26-In_2O_3 is the biggest at 1300 K, which means the sensitivity coefficient of this combination is bigger than ITO-In_2O_3 in theory.
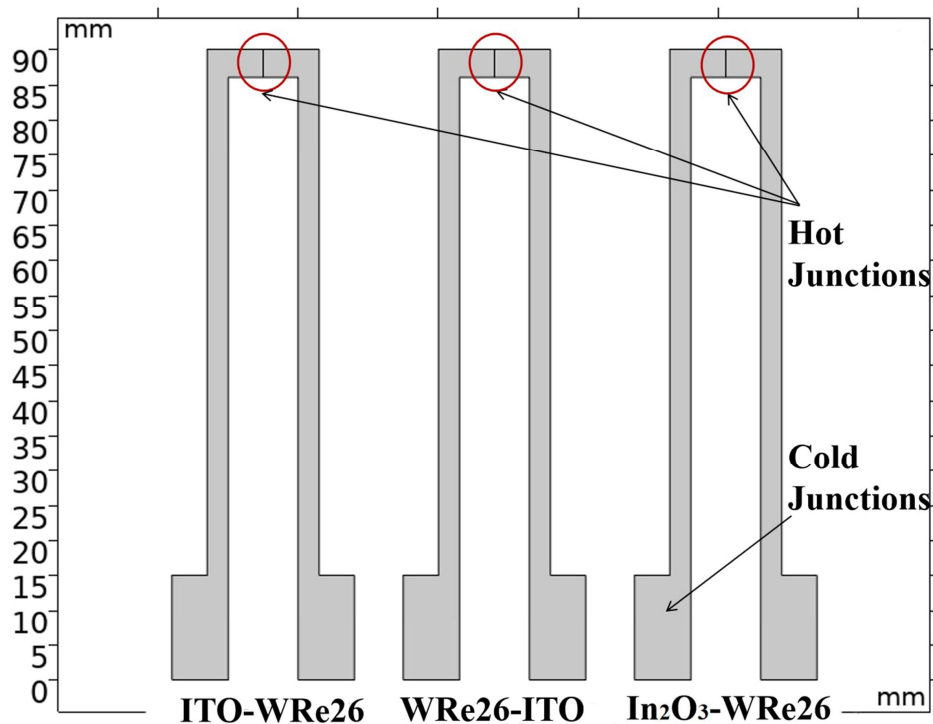

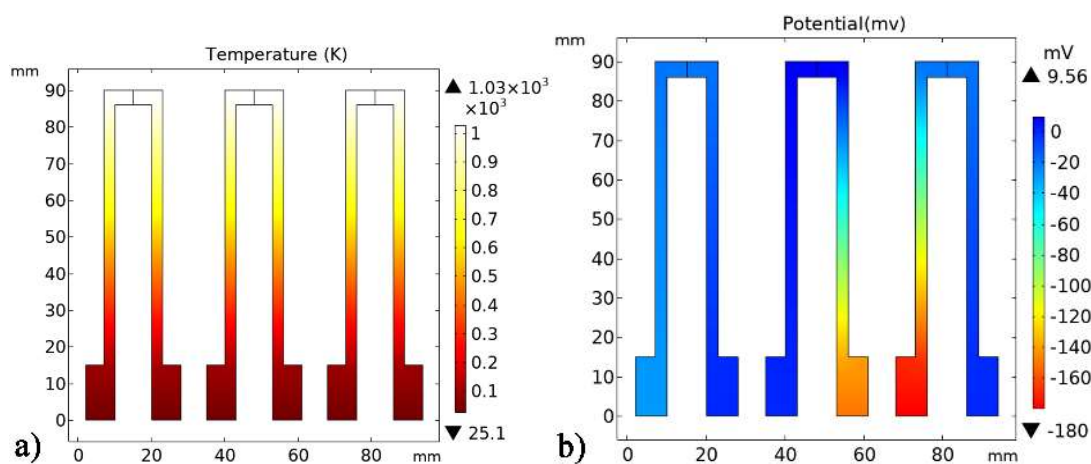**Figure 1.** Simulation model of three thermocouple combinations.

Figure 2. Simulation of three combinations. (**a**) The temperature difference distribution of thermocouples. (**b**) The thermoelectric voltage distribution.
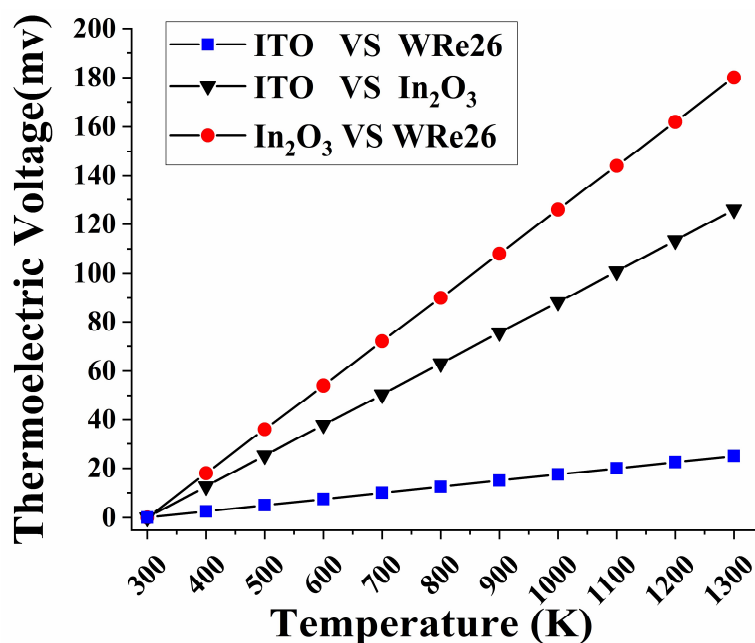

Figure 3. Thermoelectric voltage of three combinations simulation results.

3. Experiment

In order to study the effect of different annealing on the thermoelectric voltage of TFTCs, In_2O_3 film samples and WRe26-In_2O_3 TFTCs were prepared by RF magnetron sputtering. RF Magnetron sputtering technology is widely used because of the good adhesion of the films on the substrate, good thickness uniformity and high film density [29–31]. High purity WRe26 and In_2O_3 Target (purity 99.999 wt.%, diameter: 101.6 mm, and thickness: 3 mm) were been used while the distance between target and substrate was 80 mm. In Figure 4, WRe26 and In_2O_3 films were deposited on the Si_3N_4 substrate. The mass size of Si_3N_4 substrate is 30 mm × 90 mm × 3 mm, and the TFTC is 8 mm × 70 mm × 2 um.
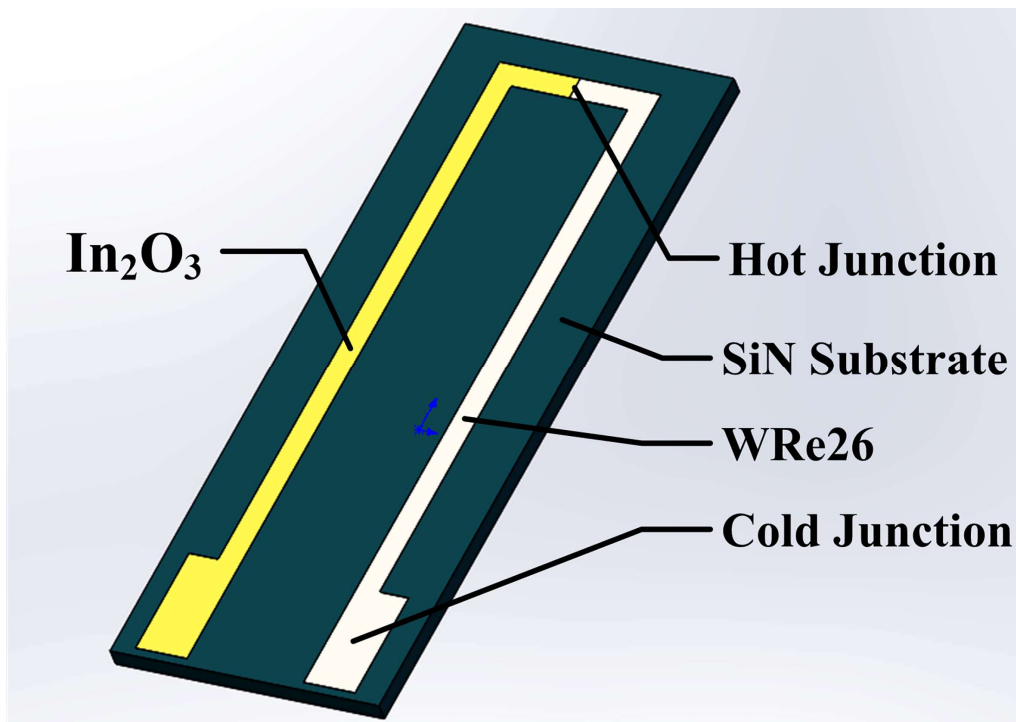
Figure 4. Structure of WRe26-In$_2$O$_3$ TFTCs.

Table 1 shows the detail sputtering parameters of the TFTCs preparation. The order of deposition of the two legs of the TFTCs were especially important. The leg of WRe26-In$_2$O$_3$ TFTCs pattern was transferred by using photolithography. In$_2$O$_3$ films deposited by magnetron sputtering for 4 h. Then, In$_2$O$_3$ films were soaked in different annealing processes. After the TFTCs were cleaned up, the WRe26 films were sputtered for 90 min with a high power of 400 w. Finally, the Al$_2$O$_3$ protective layer was covered on the sensitive layer again.

Table 1. Sputtering parameters of WRe26-In2O3 TFTCs.

Sputtering Parameters	WRe26	In$_2$O$_3$	Al$_2$O$_3$
Thickness (μm)	2	4	2
Power (W)	400	150	200
Presser (Pa)	1×10^{-6}	1×10^{-6}	5×10^{-5}
Ar (sccm)	30	60	30

The In$_2$O$_3$ films samples at different annealing processes were presented in Figure 5a. The Al$_2$O$_3$ substrate was 14 mm $\times$ 20 mm $\times$ 1 mm. The color of film samples obviously changed under different annealing processes. The crystal structure of In$_2$O$_3$ at different annealing conditions was analyzed by X-ray diffraction (XRD), X-ray photoelectron spectroscopy (XPS) was used to characterize its chemical composition. Scanning electron microscopy (SEM) was used to observe the micro-morphology of In$_2$O$_3$ at different annealing conditions, and the WRe26-In$_2$O$_3$ TFTCs were prepared to find the best annealing process by thermoelectric voltage testing (Figure 5b).
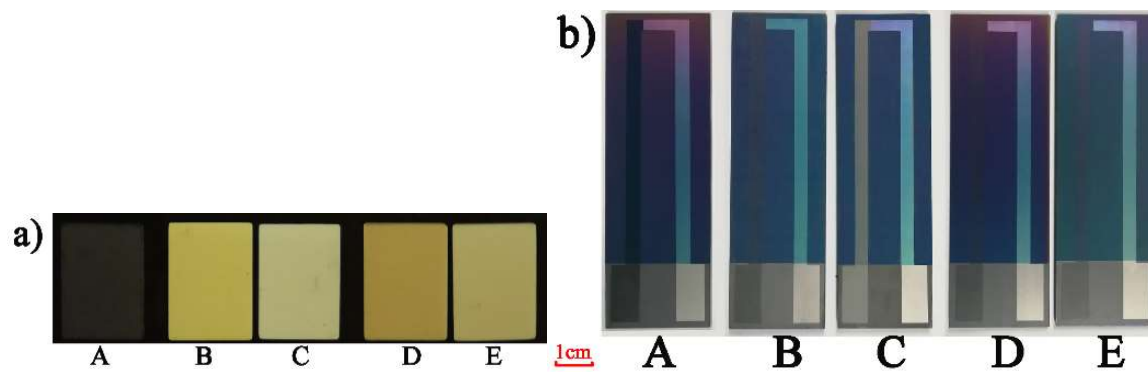
Figure 5. (**a**) Prepared In$_2$O$_3$ thin film samples at different annealing processes. (**b**) Prepared TFTCs under different annealing processes. (A: No annealing. B: 600 °Cin air for 2 h. C: 1000 °C in air for 2 h. D: 600 °C in vacuum for 2 h. E: 1000 °C in vacuum for 2 h.).

Fabricated WRe26-In$_2$O$_3$ TFTCs were static tested in muffle furnace (LHT0820, Nabertherm, Lilienthal, Germany). As shown in Figure 6, one K-type thermocouples and WRe26-In$_2$O$_3$ TFTCs were placed in the muffle furnace to get the temperature of hot junctions. Another K-type was used to monitor the cold junctions. Cold junctions of the TFTCs were cooled by circulating cold water to maintain a big temperature gradient. Then thermoelectric voltage of K-type thermocouples and the WRe26-In$_2$O$_3$ TFTCs were recorded with a data collector (Hioki, LR8410-30, Nagano, Japan).
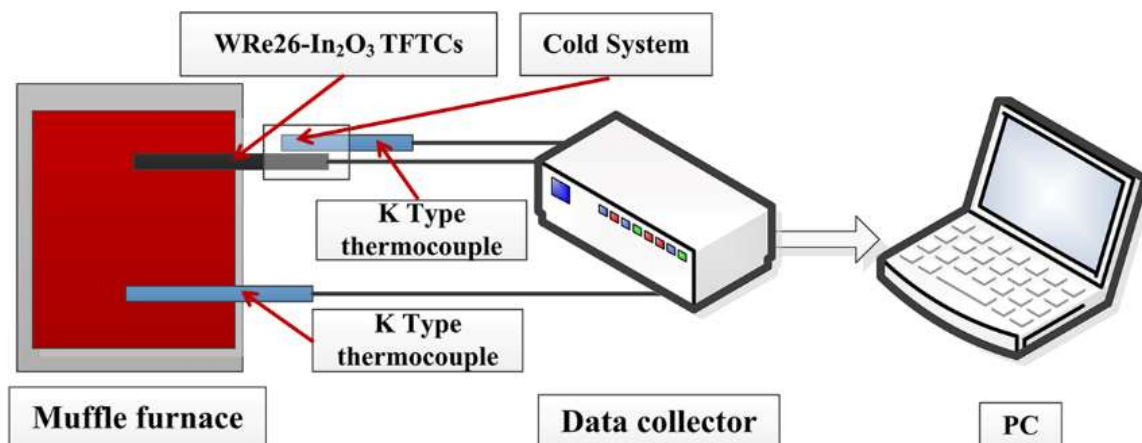

Figure 6. Thermoelectric test system of WRe26-In$_2$O$_3$ TFTCs.

4. Result and Discussion

The X-ray diffraction (XRD) patterns of In$_2$O$_3$ film samples at different annealing process were presented in Figure 7. As shown in Figure 7a, the (222) peak of In$_2$O$_3$ is very small at no annealing. With increasing of air annealing temperature, the (222) and (400) peaks of In$_2$O$_3$ were promoted a great deal, especially the (222) peak increases in the air annealing at 1000 °C. This indicates that the preferred growth of the crystal plane are (222) and (400) crystal planes. In Figure 7b, it was obvious that each peak of In$_2$O$_3$ in XRD was nearly unchanged at the anaerobic annealing processes.
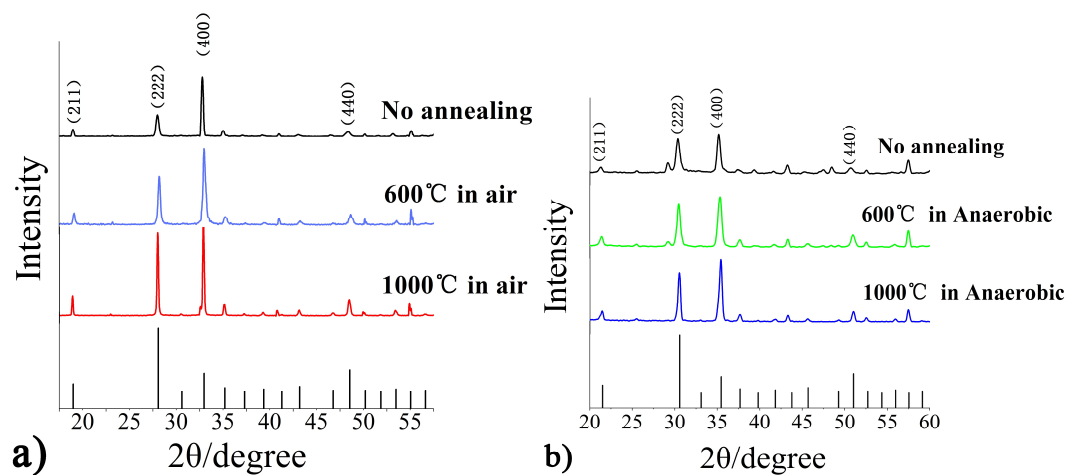
Figure 7. X-ray diffraction patterns of In$_2$O$_3$ film under different annealing processes, (**a**) Annealing process at different temperatures with air environment treatment, (**b**) Annealing process at different temperatures with vacuum treatment.

XPS was used to analyze the oxygen element in In$_2$O$_3$ films at different annealing conditions. O 1s core energy spectrum of In$_2$O$_3$ films are shown in Figure 8. The O1s spectrum of In$_2$O$_3$ films has two peaks. The binding energy of 529 eV corresponds to the O element peak and binding energy of 531 eV corresponds to the O^{2-} element peak in In$_2$O$_3$ films. The area ratio under peak of O1s (I) and O1s (II) increased after 600 °C air annealing for 2 h. It is mainly because a large amount of oxygen in the air will not enter the film at a low temperature. Instead, oxygen escaped from the film to produce more oxygen vacancies and the O^{2-} element was increased. Then, In$_2$O$_3$ films recrystallized after annealing at 1000 °C for 2 h. More oxygen entered the In$_2$O$_3$ film, and oxygen vacancy defects were reduced, causing the carrier concentration of In$_2$O$_3$ to be reduced.
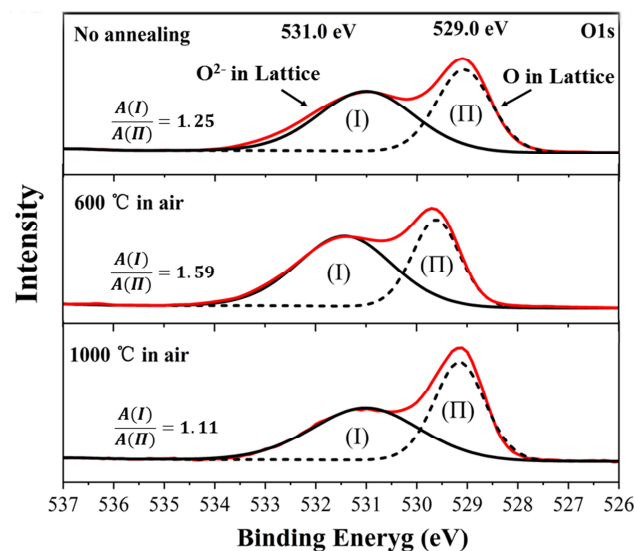

Figure 8. O1s photoelectron peaks of In$_2$O$_3$ in XPS at different annealing conditions.

Figure 9 exhibits the SEM of the In$_2$O$_3$ films under different annealing conditions. Compared to anaerobic and air annealing, as the temperature increased, the microstructures of In$_2$O$_3$ just became denser at anaerobic annealing. But the microstructures of In$_2$O$_3$ were changed significantly under air annealing. The organization grains of In$_2$O$_3$ became denser and larger, and the cellular crystals were formed at 1000 °C, implying that the oxygen entered the thin film structure at 1000 °C air annealing,

and the oxygen occupied the oxygen vacancy of the In_2O_3 films, making the conductive electrons in the In_2O_3 film decrease rapidly according to the Equation (3). As a result, the Seebeck coefficient of In_2O_3 increased.
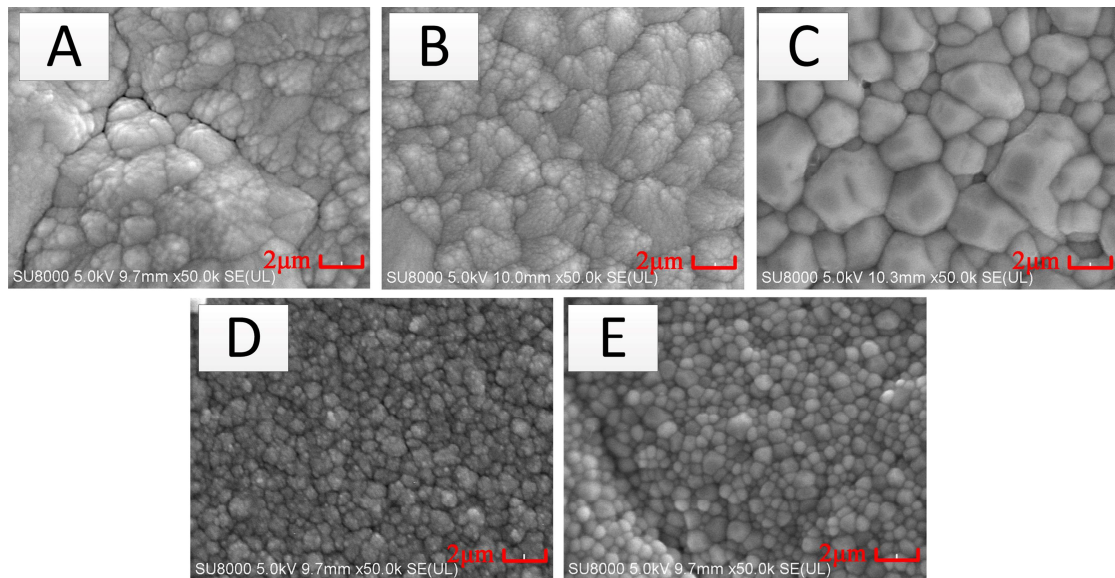

Figure 9. The SEM of In_2O_3 films under different annealing processes. (**A**: No annealing. **B**: 600 °C in air for 2 h. **C**: 1000 °C in air for 2 h. **D**: 600 °C with vacuum for 2 h. **E**: 1000 °C with vacuum for 2 h.).

To verify this phenomenon, Figure 10 shows the result of a static test of TFTCs from room temperature to 673 K at the different annealing process. It is obvious that the thermoelectric voltage was the smallest at no annealing. There were slight changes in the microstructures of In_2O_3 in 600 °C and 1000 °C anaerobic annealing. The thermoelectric voltage was significantly smaller than air annealing treatment. Thermoelectric voltage at 1000 °C air annealing was much bigger than 600 °C air annealing, which means the Seebeck coefficient of In_2O_3 films can be improved under air annealing processes, making the performance of WRe26-In_2O_3 TFTCs better.
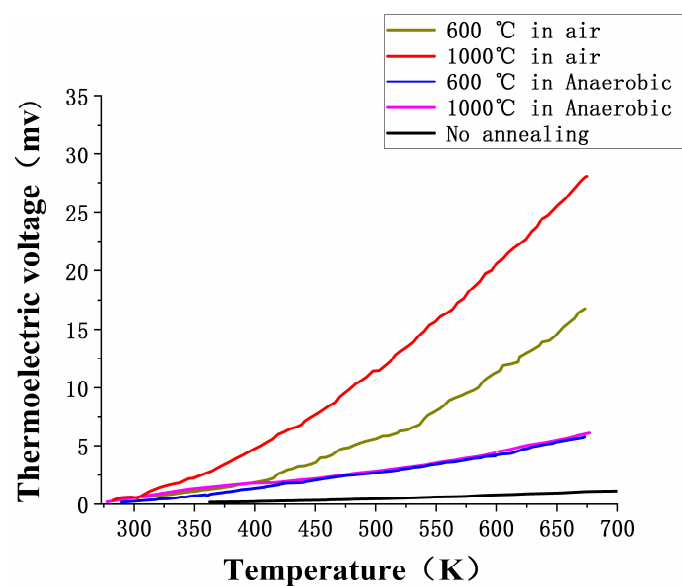

Figure 10. Thermoelectric voltage output of TFTCs.

In order to find the optimal annealing processes, the In_2O_3 films were annealed at 1000 °C for a longer time. As shown in Figure 11, with longer time in high temperature annealing, structure grains of In_2O_3 continued to grow and became more uniform, especially at 10 h. But from the test results of of WRe26-In_2O_3 TFTCs in Figure 12, it is observed that the thermoelectric voltage output is best at air annealing for 8 h. Thermoelectric voltage output for 10 h is smaller than that for 4 h. The reason was that voids appeared in the In_2O_3 films (Figure 11d), the grain boundaries of the In_2O_3 films structure become discontinuous, and the conductivity of the In_2O_3 films became poor during long duration annealing processes, although oxygen promoted the growth of tissue grains, leading to poor conductivity of the In_2O_3 film.
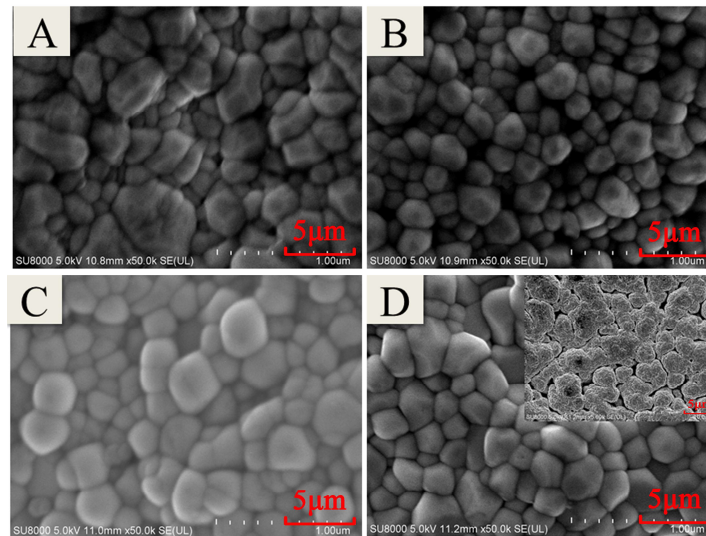

Figure 11. The SEM of In_2O_3 films under different annealing processes. (**A**: 1000 °C in air for 4 h. **B**: 1000 °C in air for 6 h. **C**: 1000 °C in air for 8 h. **D**: 1000 °C in air for 10 h.).
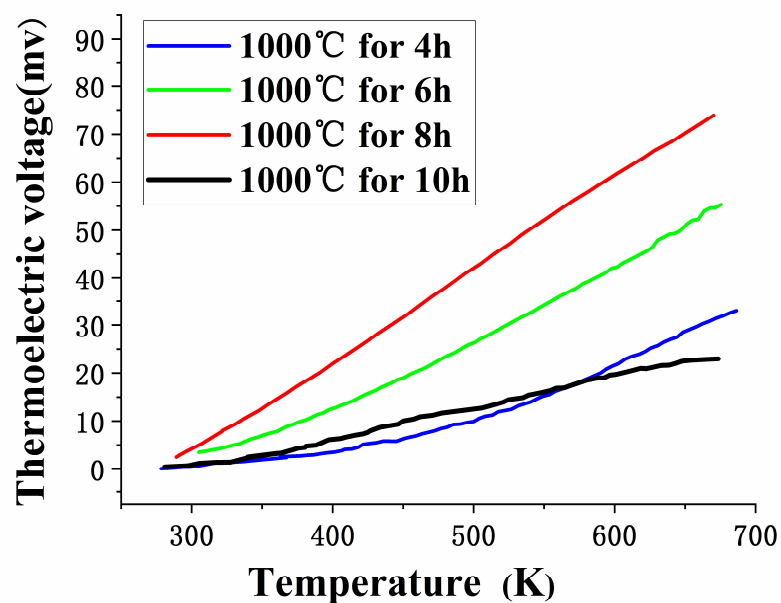

Figure 12. Thermoelectric voltage output of TFTCs.

The measured thermoelectric voltage depends on the difference between hot junction (T_h) and cold junction (T_c) and the Seebeck coefficient of the metal materials. The sensitivity coefficient (S) of thermocouples is given as:

$$S = \frac{\Delta V}{\Delta T} = \frac{\Delta V}{T_h - T_c} \tag{4}$$

where the ΔV is the thermoelectric voltage difference between the WRe26 and In$_2$O$_3$. Figure 13 shows the average sensitivity (The temperature difference was 400K) of WRe26-In$_2$O$_3$ TFTCs at different annealing. The sensitivity coefficient of the TFTCs reached 186.1 μV/K at air annealing for 8 h.
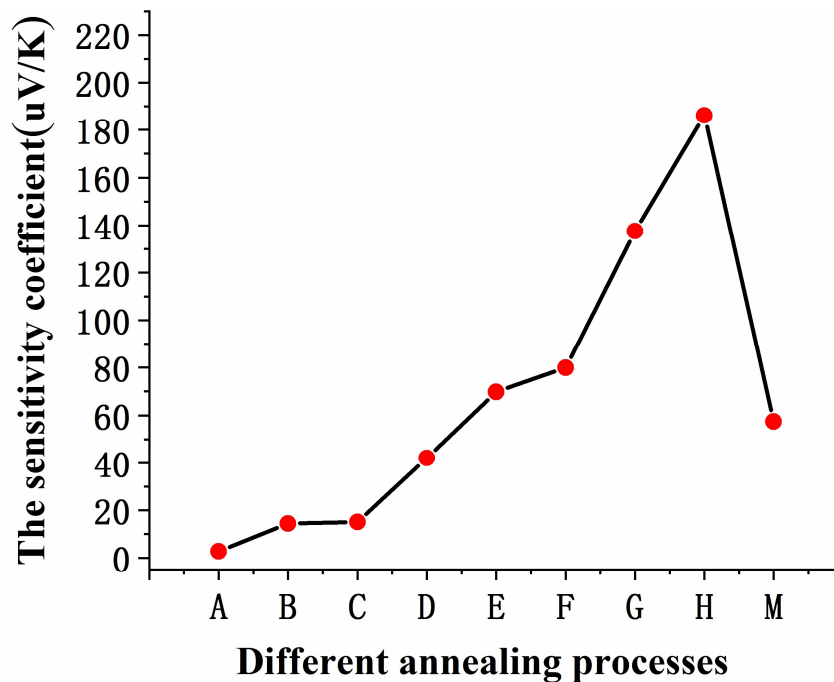

Figure 13. Average sensitivity coefficients of TFTCs at different annealing processes. (A: No annealing. B: 600 °C in air for 2 h. C: 1000 °C in air for 2 h. D: 600 °C with vacuum. E: 1000 °C with vacuum. F: 1000 °C in air for 4 h. G: 1000 °C in air for 6 h. H: 1000 °C in air for 8 h. M: 1000 °C in air for 10 h.).

Prepared WRe26-In$_2$O$_3$ TFTC was static calibrated in a high temperature after the optimal annealing process was determined. Figure 14 shows the temperature stability test of TFTC in muffle furnace. The WRe26-In$_2$O$_3$ TFTC and K-type thermocouples were raised from room temperature to 773 K and kept for two hours, and heated to 1000 K for twenty minutes. The heating rate was set at 10 °C/min. Then, TFTC was naturally cooled to room temperature. Figure 15 is a static thermoelectric voltage curve of WRe26-In$_2$O$_3$ TFTCs with the temperature difference up to 612.9 K. The hot junction of the thermocouple was 1000 K (the temperature of cold junction was 387.1 K), the thermoelectric voltage reached 123.6 mv. The average sensitivity coefficient was 201.6 μV/K. We have found the optimal annealing process at this magnetron sputtering process, but the Seebeck coefficient of In$_2$O$_3$ in the literature is about −200 μV/K, and the Seebeck coefficient of WRe26 is about 20 μV/K. So the sensitivity of the WRe26-In$_2$O$_3$ TFTCs is about 220 μV/K in theory. There was a little difference between the prepared TFTC and the theoretical thermoelectric output. This is mainly because the source of the In$_2$O$_3$ target was different, and so the Seebeck coefficient of In$_2$O$_3$ was also a little different. The Seebeck coefficient of In$_2$O$_3$ was highly affected by the quality In$_2$O$_3$ film.
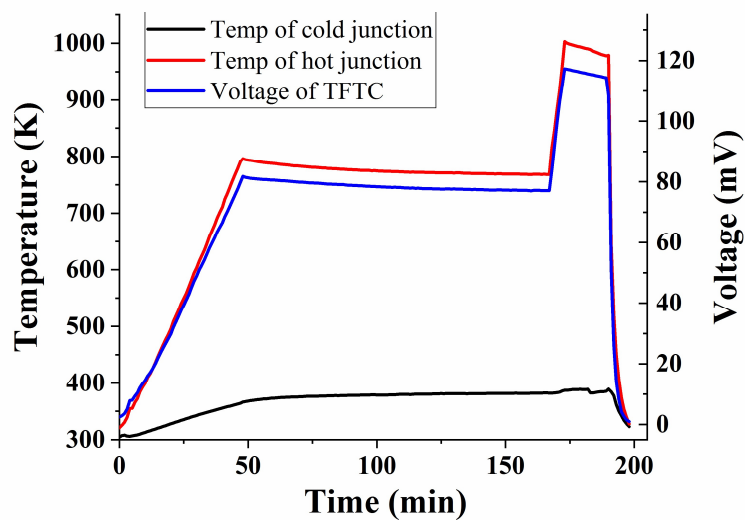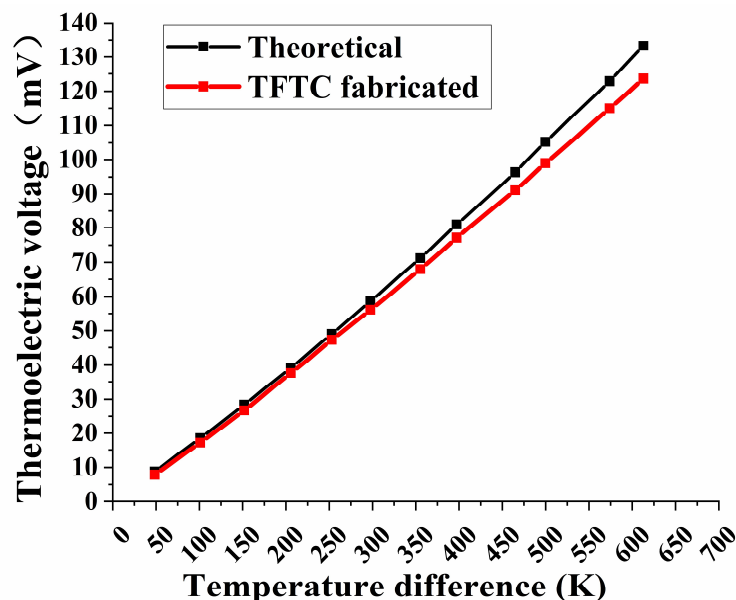
Figure 14. Thermoelectric voltage of WRe26-In$_2$O$_3$ TFTCs.

Figure 15. Static test thermoelectric voltage and theoretical curve of WRe26-In$_2$O$_3$ TFTCs.

5. Conclusions

In this study, a WRe26-In$_2$O$_3$ TFTC was reported. The WRe26-In$_2$O$_3$ TFTCs were successfully fabricated on the Si$_3$N$_4$ substrate by magnetron sputtering in order to improve the thermoelectric performance of the thermocouple. The properties of In$_2$O$_3$ films and the thermoelectric voltage properties of the WRe26-In$_2$O$_3$ TFTCs under different annealing processes were studied. The properties of In$_2$O$_3$ films at different annealing processes were analyzed by SEM, XRD, and XPS. The optimal annealing process of the TFTCs under this sputtering method was proposed. The WRe26-In$_2$O$_3$ TFTCs had ideal performance at the 1000 °C air annealing for 8 h. It was achieved that the average sensitivity of the WRe26-In$_2$O$_3$ TFTCs could reach 201.6 μV/K at a temperature difference of 612.9 K, which can maintain a stable output for 2 h at 773 K and 20 min for 1000 K.

Author Contributions: Conceptualization, B.T. and Y.L.; methodology, B.T. and Y.L.; software, Z.Z.; validation, Z.Z.; formal analysis, Y.L.; investigation, Z.L., Q.M., P.S., D.L., Q.L.; data curation, Y.L.; writing—original draft preparation, Y.L.; supervision, B.T., L.Z.; project administration, B.T. and Z.J. All authors have read and agreed to the published version of the manuscript.

Conflicts of Interest: The authors declare no conflict of interest. The funders had no role in the design of the study.

References

1. Basti, A.; Obikawa, T.; Shinozuka, J. Tools with built-in thin film thermocouple sensors for monitoring cutting temperature. *Int. J. Mach. Tools Manuf.* **2007**, *47*, 793–798. [CrossRef]
2. Majumdar, A.; Lai, J.; Chandrachood, M. Thermal imaging by atomic force microscopy using thermocouple cantilever probes. *Rev. Sci. Instrum.* **1995**, *66*, 3584. [CrossRef]
3. Leboek, J.; Ali, S.T.; Moller, P. Quantification of in situ temperature measurements on a PBI-based high temperature PEMFC unit cell. *Int. J. Hydrog. Energy* **2010**, *35*, 9943–9953. [CrossRef]
4. Aniolek, E.; Gregg, O.J. Thin film thermocouples for advanced ceramic gas turbine engines. *Surf. Coat. Technol.* **1994**, *68*, 70–75. [CrossRef]
5. Gregory, O.J.; Amani, M. Stability and microstructure of indium tin oxynitride thin films. *J. Am. Ceram. Soc.* **2012**, *2*, 705–710. [CrossRef]
6. ASTM. *E230/E230M-12, Standard Specification and Temperature Electromotive Force (emf) Tables for Standardized Thermocouples*; ASTM International: West Conshohocken, PA, USA, 2012.
7. Ren, J.; Donovan, D.; Watkins, J. The surface eroding thermocouple for fast heat flux measurement in DIII-D. *Rev. Sci. Instrum.* **2018**, *2018. 89*, 10J122. [CrossRef]
8. Chen, Y.Z.; Jiang, H.C. Film thickness influences on the thermoelectric properties of NiCr/NiSi thin film thermocouples. *Mod. Phys. Lett. B* **2013**, *14*, 1350103. [CrossRef]
9. Tougas, I.M.; Gregory, O.J. Thin film platinum–palladium thermocouples for gas turbine engine applications. *Thin Solid Films* **2013**, *539*, 345–349. [CrossRef]
10. Chen, Y.Z.; Jiang, H.C.; Jiang, S.W.; Liu, X.Z.; Zhang, W.L. Thin film thermocouples for surface temperature measurement of turbine blade. *Adv. Mater. Res.* **2014**, *873*, 420–425. [CrossRef]
11. Guo, H.; Jiang, J.Y.; Liu, J.X.; Nie, Z.H.; Ye, F.; Ma, C.F. Fabrication and Calibration of Cu-Ni thin film thermocouples. *Adv. Mater. Res.* **2012**, *512*, 2068–2071. [CrossRef]
12. Wrbanek, J.D.; Fralick, G.C. Development of thin film ceramic thermocouples for high tempe-rature environments. In Proceedings of the 40th AIAA/ASME/SAE/ASEE Joint Propulsion Conference and Exhibit. American Institute of Aeronautics and Astronautics, Fort Lauderdale, FL, USA, 11–14 July 2004.
13. Vedula, R.; Desu, S.B.; Fralick, G.C. Thin film TiC/TaC thermocouples. *Thin Solid Films* **1999**, *342*, 214–220.
14. Kreider, K. Thin Film High Temperature Silicide Thermocouples. U.S. Patent 5,474,619, 12 December 1995.
15. Liu, Y.; Ren, W.; Shi, P.; Liu, D.; Liu, M.; Jing, W.; Tian, B.; Ye, Z.; Jiang, Z. Preparation and thermal volatility characteristics of In_2O_3/ITO thin film thermocouple by RF magnetron sputtering. *AIP Adv.* **2017**, *7*, 115025. [CrossRef]
16. Chen, X.; Gregory, O.J. Thin-film thermocouples based on the system In_2O_3–SnO_2. *J. Am. Ceram. Soc.* **2011**, *94*, 854–860. [CrossRef]
17. Liu, Y.; Ren, W.; Shi, P.; Liu, D.; Zhang, Y.; Liu, M.; Lin, Q.; Tian, B.; Jiang, Z. Microstructure and thermoelectric properties of In2O3/ITO thin film thermocouples with Al_2O_3 protecting layer. *J. Mater. Sci. Mater. Electron.* **2018**, *30*, 1786–1793. [CrossRef]
18. Zhao, X.H.; Ying, K. Stability and thermoelectric properties of ITON: Pt thin film thermocouples. *J. Mater. Sci. Mater. Electron.* **2016**, *27*, 1725–1729. [CrossRef]
19. Liu, Y.L.; Ren, W. A highly thermostable In_2O_3/ITO thin film thermocouple prepared via screen printing for high temperature measurements. *Sensors* **2018**, *18*, 958. [CrossRef]
20. Zhao, X.; Li, H.; Chen, Y. Preparation and thermoelectric characteristics of ITO/Pt thin film thermocouples on Ni-based superalloy substrate. *Vacuum* **2016**, *140*, 116–120. [CrossRef]
21. Zhang, Y.; Cheng, P. ITO film prepared by ion beam sputtering and its application in high-temperature thermocouple. *Vacuum* **2017**, *146*, 31–34. [CrossRef]
22. Tian, B.; Zhang, Z. Tungsten-rhenium thin film thermocouples for sic-based ceramic matrix composites. *Rev. Sci. Instrum.* **2017**, *88*, 015007. [CrossRef]

23. Zhang, Z.; Tian, B. Thermoelectric Characteristics of Silicon Carbide and Tungsten-Rhenium-Based Thin-Film Thermocouples Sensor with Protective Coating Layer by RF Magnetron Sputtering. *Materials* **2019**, *12*, 1981. [CrossRef]

24. Zhang, Z. Research on Measurement and Process of Tungsten-Rhenium Thin Film Thermocouples Sensor. In Proceedings of the 2018 IEEE 13th Annual International Conference on Nano/Micro Engineered and Molecular Systems (NEMS), Singapore, 22–26 April 2018; pp. 139–142.

25. Molki, A. Simple demonstration of the seebeck effect. *Sci. Educ. Rev.* **2010**, *9*, 525–536.

26. Mcaleer, J.F.; Moseley, P.T.; Bourke, P. Tin dioxide gas sensors: Use of the seebeck effect. *Sens. Actuators* **1985**, *8*, 251–257. [CrossRef]

27. Jonker, G. The Application of Combined Conductivity and Seebeck Effffect Plots for the Analysis of Semiconductor Properties. *Philips Res. Rep.* **1968**, *23*, 131–138.

28. Ellmer, K.; Mientus, R. Carrier Transport in Polycrystalline ITO and ZnO:Al II: The Inflfluence of Grain Barriers and Boundaries. *Thin Solid Films* **2018**, *516*, 5829–5835. [CrossRef]

29. Ellmer, K. Magnetron sputtering of transparent conductive zinc oxide: Relation between the sputtering parameters and the electronic properties. *J. Phys. D* **2000**, *33*, 4. [CrossRef]

30. Kelly, P.J. Magnetron sputtering: A review of recent developments and applications. *Vacuum* **2000**, *56*, 159–172. [CrossRef]

31. Zhang, Z.; Tian, B.; Du, Z. Impact of magnetron sputtering parameters on thermoelectric properties of tungsten-rhenium thin-film thermocouples sensor. *IEEE Sens. J.* **2018**, *24*, 9896–9901. [CrossRef]